CFD MODELLING OF SWIRLING DEVICE TO STUDY BEND EROSION RATE AT DIFFERENT BEND ANGLES IN PNEUMATIC CONVEYING SYSTEM

Reference NO. IJME 1342, DOI: 10.5750/ijme.v1i1.1342

Bharat Singh Yadav*, **Rajiv Chaudhary** and **R.C. Singh**, Department of Mechanical Engineering, Delhi Technological University, Delhi 110042, India

* Corresponding author. Bharat Singh Yadav (Email): bharat_2k19phdme22@dtu.ac.in

KEY DATES: Submission date: 21.11.2023 / Final acceptance date: 26.02.2024 / Published date: 12.07.2024

SUMMARY

Bend Erosion problems were found mostly common in pneumatic conveying plants. Swirling of particles before striking the bend has been noted as the best solution to minimize bend erosion rate. CFD k-w model in Ansys was applied to analyze mild steel bend erosion in the pipeline by pneumatically conveyed particles with a motor-operated swirling device. A part of the pipe before the bend is rotated at different velocities in different elbow geometries from 15° to 90° elbows. A combination of Eulerian and Lagrangian methods were utilized to track particles. Mathematical modelling of the swirling of particles on bent surfaces is taken into consideration with different elbow angle. The bend erosion rate was mitigated due to the swirling of particles. Different velocities and parameters are taken to evaluate the results. At different bend angles erosion rate is different and the swirling device minimizes the bend erosion rate.

KEYWORDS

Swirling device, Mean effective particle (mep) size, Erosion rate

NOMENCLATURE

υ	Kinematic viscosity (N s m^{-2})
ρ	Density of water (kg m^{-3})
P	Pressure (N m^{-2})
v	Velocity (m/sec)
m	Mass Flow Rate kg/sec
ϕ	Form Factor
PCS	Pneumatic Conveying System
mep	Mean Effective Particle Size of Silica, µm

1. INTRODUCTION

Different types of bends like Metric (M) bends, sharp bends (S), and other types of different angle bends are used to convey powder-type particles. G. Arun [1] discussed the comparison of 90° S and M bends for erosion rate. Differences in the swirl flow induced at the pipe assembly's outlet were reported. Computational Fluid Dynamics (CFD) modeling on Ansys has been utilized to find the bend erosion rate in a pneumatic conveying system. A computational fluid dynamics-based erosion prediction model and its application to 3D double elbows were presented by Li et al. [2]. The numerical flow visualization results help in understanding the detailed flow characteristics in the 90°-S and 90°-M pipe bends. Wall shear stresses were observed in S bend pipe assemblies because of abrupt sharp flow turning which produces higher pressure drops. It is evident that several experimental and computational/numerical studies were conducted in smooth pipe bends with constant radii. The appropriate bend geometric parameters were found and reported using computer simulations. Jiang et al. [3] used the volume of fluid (VOF) model in conjunction with the continuous surface stress (CSS) model to simulate the core annular of non-Newtonian oil and water flow through the rectangular return bends. Conversely, mitered bends created by combining two or more pieces of sheet metal pipe segments are frequently utilized in a variety of industrial settings when a sharp turn in the flow is required. When there is not enough room for a smooth, constant-radius bend, these mitered bends are utilized. Hiroshi and associates using turbulent flow through a 90° pipe elbow in a range of moderately high Reynolds numbers between 14,000 and 34,000 by wall-resolved large-eddy simulation (LES) and multiple Reynolds-averaged Navier-Stokes (RANS) models, studied computationally to demonstrate advantages and disadvantages of different computational methods for the considered case. The RANS models utilized in this investigation comprise the fundamental low Reynolds number k-model [4]. A laminar non-Newtonian pseudoplastic power law model was employed by Bandyopadhyay et al. [5] to simulate non-Newtonian liquid

flow through elbows. The Eulerian-Eulerian technique has been used for two-phase flow. The Differential Stress Model (DSM) is utilized in conjunction with the standard form of the wall function (SWF), the Analytical Wall Function (AWF), and the Numerical Wall Function (NWF) used by Rohrig et al. [6]. While the Nusselt number predictions along the outer wall after the bend exit have significantly improved it has not demonstrated any other notable predictive advantages over the other DSM models. Li Wei et al. [7] used the RNG k-e model, the realizable k-e model, and the Reynolds Stress Model (RSM) for numerical analysis of the effect of flow Reynolds number on the curvature ratio (d) for the hydraulic oil flow in a smooth 90° bend. Many investigators performed numerical calculations of pipe bends. A square cross-sectioned U bend with a steep curvature ratio was used to model the complex flow by Song and Amano [11]. To anticipate the behaviour of turbulent flow, the scientists employed a non-linear low Re k-x model to electronic systems by conducting unsteady, laminar, flow, and thermal simulations in a two-dimensional abrupt turning 180° bends (without any joint). Homicz [9] used Ansys Fluent to simulate flow in a smooth CFD Simulation.

Three-dimensional, incompressible, steady-state computational fluid dynamic investigations were conducted to comprehend the intricate flow behaviour in these pipe designs. Ansys Fluent, a finite volume method (FVM) based solver, a commercial flow simulation tool, was utilized for this purpose. CATIA V5 was used as a pre-processing tool to model the pipe bends and mesh the computational domain.

1.1 CAD MODEL SETUP

Two 8-camera models were created for this investigation. Without a whirling device, cases 1 through 4, and with one, cases 5 through 8. With the aid of Catia software, the CAD model was created. Table 1 shows the Ansys model dimensions taken into consideration.

1.2 MESHING

In ANSYS CFD modelling, nodes and elements are created to occupy the entire flow volume, forming a mesh. Each cell within this mesh represents a distinct region

Table 1. Model dimensions

	Dimensions
H	1000mm
V	500mm
Swirling device length	500mm
Diameter of Pipe	51mm
Angle	90 degrees

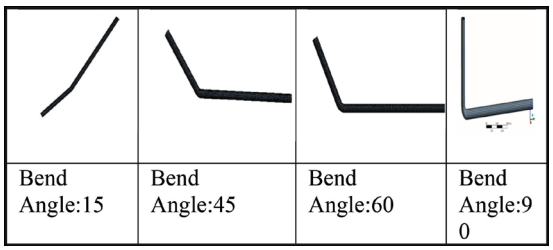

Fig.1. Mesh model

that characterizes the local flow. Mathematical equations, which govern the flow physics, are subsequently applied to each cell in the mesh. The quality of this mesh is of utmost importance as it directly impacts the reliability of the solutions obtained and ensures numerical stability. In the current study, the CAD model of the pipe bend was divided into 13,320 nodes and 11,456 elements. The mesh model is shown in Fig. 1.

1.3 CFD SIMULATION MODEL

First define the Steady Flow Model for the study of four bend Designs in the XZ H-plane with gravity in the Y direction is 9.81m/s^2. The working fluid is the main important factor in CFD in this study air as the working fluid for the study.

The defined temperature is 27^{o}C, the specified air density is 1.293kg/m^3, and the specified viscosity is 1.810-5 kg.m^{-1}. s^{-1}. Choosing inlet type as velocity inlet and inlet velocity on the system was U = 23.11 m/s CFD boundary Conditions are shown in Table 2.

A standard k-two equations turbulence model is used for simmulation. This model is constructed using transport equations for both turbulence kinetic energy (k) and dissipation rate (ε). It's important to note that this model applies only to fully turbulent flows. To depict wall-bounded turbulent flows, we utilize scalable wall functions. Notably, our turbulence model has undergone

Table 2. CFD boundary condition

Boundary condition	
Rotary feeder speed	125 RPM
Pressure of root blower	1 bar
Free air CFM	100CFM=0.0472 m^3/sec
Cycle time	45*60=2700 sec
Mass flow rate (Particle)	0.074kg/sec
Mass flow rate (Air)	0.0547kg/sec
Inlet velocity (Air)	23.11m/sec
Swirling device speed	100rpm,
Distance of swirling device bend	0.5 meters

revisions to allow for the resolution of the viscosity-affected region, encompassing the viscous sublayer, through a mesh that extends to the wall. This approach enhances the accuracy of our simulations near the boundary surfaces.

1.4 SIMULATION STEP OF WORKING

Step 1 Identification of the Flow Issue.

Step 2 Design model for Flow domain.

Step 3 Set the Boundary and Initial Conditions.

Step 4 CFD Meshing.

Step 5 Define Simulation Strategy for CFD.

Step 6 Define the Input files and Parameters.

Step 7 Start the Simulation.

Step 8 Monitor on the Simulation's progress.

Step 9 To obtain the results do post process the simulation.

Step 10 Results Comparison.

Step 11 Examination of sensitivity.

Step 12 Document.

1.5 CFD GOVERNING EQUATIONS

CFD governing equations enhances are explained below

1.5.1 Viscous -SST K-omega

The SSk-turbulence model, first developed by Menter in 1993, stands as a prominent example of a two-equation eddy-viscosity model. In the field of turbulence modeling, the pursuit of a versatile approach has led to the creation of the shear stress transport (SST) model, which combines various advantages effectively. The k- model within the SST serves as a robust Low-Re turbulence model, eliminating the need for additional damping functions by incorporating a k- formulation within the inner regions of the boundary layer. What sets this model apart is its unique ability to extend its applicability to the wall, encompassing even the viscous sub-layer. This distinguishes it from conventional k- k-models, known for their sensitivity to free-stream turbulence conditions at the inlet. The SST formulation seamlessly transitions to k- k-behavior in the free stream, making it a preferred choice for researchers dealing with complex pressure gradients and separated flows.

$$\frac{\partial \omega}{\partial t}+U_j\frac{\partial \omega}{\partial x_j}=\alpha S^2-\beta\omega^2+\frac{\partial}{\partial x_j}\left[\left(\nu+\sigma_\omega \nu_T\right)\frac{\partial \omega}{\partial x_j}\right] +2\left(1-F_1\right)\sigma_{\omega 2}\frac{1}{\omega}\frac{\partial k}{\partial x_i}\frac{\partial \omega}{\partial x_i}$$

$$\nu_T=\frac{a_1 k}{\max\left(a_1\omega,\ SF_2\right)}$$

However, it's important to note that in scenarios involving high normal strain, such as stagnation and rapid acceleration, the SST k- k-model may exhibit a slight inclination to produce somewhat higher turbulence levels. Nevertheless, this tendency is considerably less pronounced compared to a typical k- k-model. The widespread acceptance and adoption of the SST k- k model within the scientific community underscore its effectiveness in addressing a wide array of turbulent flow situations.

1.5.1.1 Kinematic Eddy Viscosity

$$\nu_T=\frac{a_1 k}{\max\left(a_1\omega,\ SF_2\right)}$$

1.5.1.2 Turbulence Kinetic Energy

$$\frac{\partial k}{\partial t}+U_j\frac{\partial k}{\partial x_j}=P_k-\beta^* k\omega+\frac{\partial}{\partial x_j}\left[\left(\nu+\sigma_\omega \nu_T\right)\frac{\partial k}{\partial x_j}\right]$$

1.5.1.3 Specific Dissipation Rate

$$\frac{\partial \omega}{\partial t}+U_j\frac{\partial \omega}{\partial x_j}=\alpha S^2-\beta\omega^2+\frac{\partial}{\partial x_j}\left[\left(\nu+\sigma_\omega \nu_T\right)\frac{\partial \omega}{\partial x_j}\right] +2\left(1-F_1\right)\sigma_{\omega 2}\frac{1}{\omega}\frac{\partial k}{\partial x_i}\frac{\partial \omega}{\partial x_i}$$

1.5.1.4 Closure Coefficients and Auxiliary Relations

$$F_2=\tanh\left[\left[max\frac{2\sqrt{k}}{\beta^*\omega y},\frac{500\nu}{y^2\omega}\right]\right]^2$$

$$P_k=\min\left(\tau_{ij}\frac{\partial U_i}{\partial x_j},10\beta^* k\omega\right)$$

$$F_1=\tanh\left\{\left\{\min\left[\max\left(\frac{\sqrt{k}}{\beta^*\omega y},\frac{500\nu}{y^2\omega}\right),\frac{4\sigma_{\omega 2}k}{CD_{k\omega}y^2}\right]\right\}^4\right\}$$

$$CD_{k\omega}=\max\left(2\rho\sigma_{\omega 2}\frac{1}{\omega}\frac{\partial k}{\partial x_j}\frac{\partial \omega}{\partial x_i},10^{-10}\right)$$

$$\phi = \phi_1 F_1 + \phi_2 (1 - F_1)$$

$$\alpha_1 = \frac{5}{9}, \alpha_2 = 0.44$$

$$\beta_1 = \frac{3}{40}, \beta_2 = 0.0828$$

$$\beta^* = \frac{9}{100}$$

$$\sigma_{k1} = 0.85, \sigma_{k2} = 1$$

$$\sigma_{\omega 1} = 0.5, \sigma_{\omega 2} = 0.856$$

1.5.2 Discrete Phase Modeling

In our modeling, we implement the Euler-Lagrange method to manage the discrete phase. This approach involves tracking individual particles as they move through the predicted flow field, focusing on the dispersed phase, while treating the fluid phase as a continuous medium during the solution of the Navier-Stokes equations. It's worth noting that the dispersed phase and the fluid phase can exchange mass, energy, and momentum, as highlighted in reference [7]. In our research, we utilize sand as the discrete phase, which possesses specific properties, including a density of 2500 kg/m³, a flow rate of 0.1 kg/s, and a particle diameter of 1000 µm. To account for the non-spherical shape of these sand particles, we incorporate a non-spherical drag law, as described in the same reference [7].

In our study, we use sand as the discrete phase, with specific properties such as a density of 2500 kg/m³, a flow rate of 0.1 kg/s, and a particle diameter of 1000 µm. To accommodate the non-spherical shape of these sand particles, we employ a non-spherical drag law, as described in the same reference [7].

$$C_D = \frac{24}{Re_D}.\left(1 + b_1.Re_D^{b_2}\right) + \frac{b_3.Re_D}{b_4 + Re_D} \quad (4)$$

where: C_D represents the drag coefficient and Re_D the Reynolds number.

The values for the b1, b2, b3 and b4 coefficients are calculated as follows:

$$b_1 = \exp\left(2.3288 - 6.4581\phi + 2.4486\phi^2\right) \quad (5)$$

$$b_2 = 0.0964 + 0.5565\phi \quad (6)$$

$$b_3 = \exp\begin{pmatrix} 4.905 - 13.8944\phi \\ +18.4222\phi^2 - 10.2599\phi^3 \end{pmatrix} \quad (7)$$

$$b_4 = \exp\begin{pmatrix} 1.4681 + 12.2584\phi \\ -20.7322\phi^2 + 15.8855\phi^3 \end{pmatrix} \quad (8)$$

$$\phi = \frac{s}{S} \quad (9)$$

where:

ϕ stands for the form factor,

S is the actual surface area of the particle, while s is the surface area of a sphere with the same volume as the particle.

For the CFD analysis, a sand particle form factor of = 0.9 was chosen.

2. RESULTS AND DISSCUSSION

As per the Computational fluid dynamic result, the maximum erosion rates in mm/year for pipe bends with density

ρ = 7850 Kg/m³ are shown in Table 3.

Case-1 Particle size 200 and without swirling device at an angle of 15 degrees.

In case-1 particle size was 200µm. The velocity in this case 13 m/s. pipe total erosion rate is 5.0mm/year. The CFD results contours are shown in Fig. 2.

Table 3. CFD results

Particle size	Mechanism	Parameter	Unit	Angle of Bend			
				15°	45°	60°	90°
200	Swirling device with (100 rpm)	Erosion rate	mm/year	2.5	3.3	3.5	4.0
		Velocity	m/s	25	26	29	68.7
	without swirling device	Erosion rate	mm/year	5	6.5	7.2	8.0
		Velocity	m/s	13	15	18	31.3

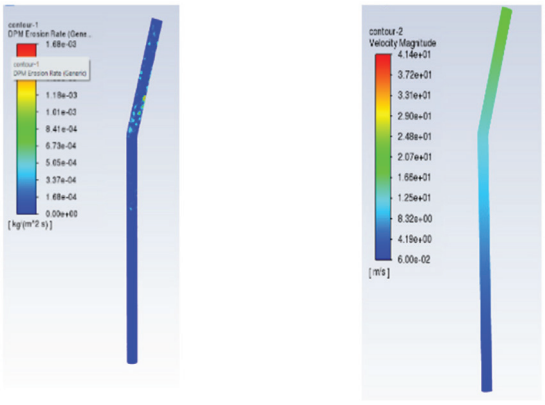

Fig.2. Erosion rate and velocity at 200 µm particle size without swirling device

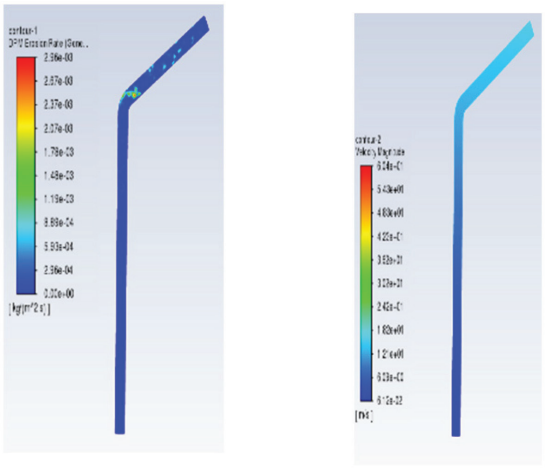

Fig.4. Erosion rate and velocity at 200 µm particle size with swirling device

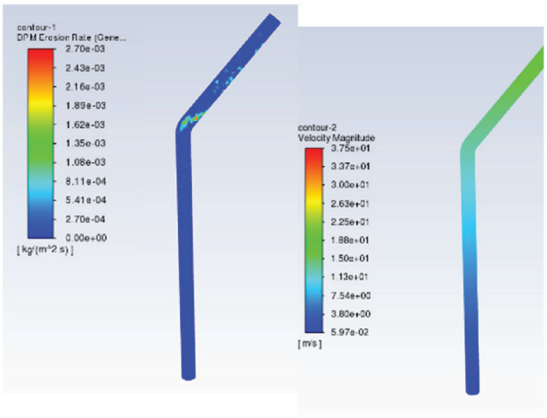

Fig.3. Erosion rate and velocity at 200 µm particle size without swirling device

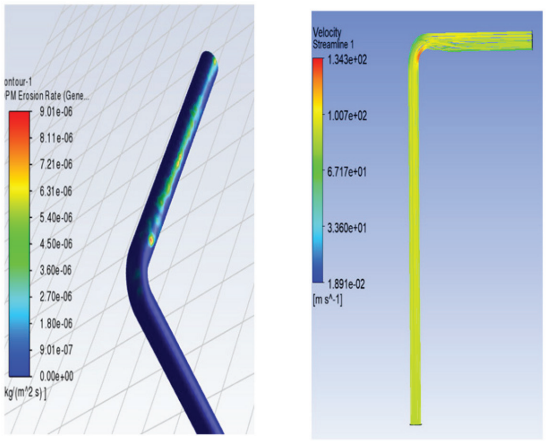

Fig.5. Erosion rate and velocity at 200 µm particle size without swirling device

Case-2 Particle size 200 and without swirling device at angle 45 degree.

In case-2 particle size was 200µm. The velocity in this case 15 m/s. pipe total erosion rate is 3.3mm/year. The CFD results contours are shown in Fig. 3.

Case-3 Particle size 200 and without swirling device at an angle of 60 degrees.

In case-3 particle size was 200µm. The velocity in this case 18 m/s. pipe total erosion rate is 7.2mm/year. The CFD results contours are shown in Fig. 4.

Case-4 Particle size 200 and without swirling device at an angle of 90 degrees.

In case-4 particle size was 200µm. The velocity in this case increases up to 31.3m/s. pipe total erosion rate is 8.0mm/year. The CFD results contours are shown in Fig. 5.

Case-5 Particle size 200 and with swirling device. 100rpm at 15 degree.

In case-5 particle size was 200µm. The velocity in this case 25 m/s. pipe total erosion rate is 2.5 mm/year. The CFD results contours are shown in Fig. 6.

Case-6 Particle size 200 and with swirling device. 100rpm at 45 degree.

In case-6 particle size was 200µm. The velocity in this case 26 m/s. pipe total erosion rate is 3.3mm/year. The CFD results contours are shown in Fig. 7.

Case-7 Particle size 200 and with swirling device. 100rpm at 60 degree.

In case-7 particle size was 200µm. The velocity in this case 26 m/s. pipe total erosion rate is 3.5mm/year. The CFD results contours are shown in Fig. 8.

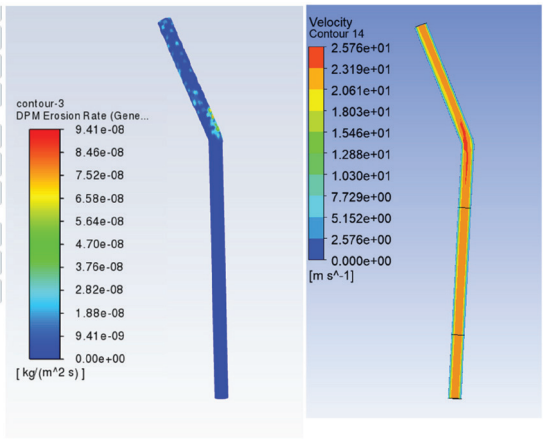

Fig. 6. Erosion rate and velocity at 200 µm particle size with swirling device

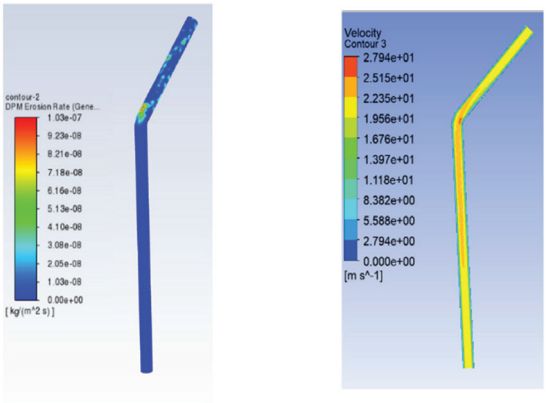

Fig. 7. Erosion rate and velocity at 200 µm particle size with swirling device

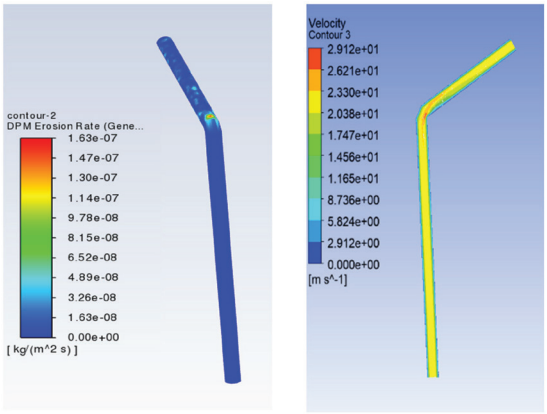

Fig. 8. Erosion rate and velocity at 200 µm particle size with swirling device

Case-8 Particle size 200 and with swirling device. 100rpm at 90 degree.

In case-8 particle size was 200µm. The velocity in this case 68 m/s. pipe total erosion rate is 5mm/year. The CFD results contours are shown in Fig. 9.

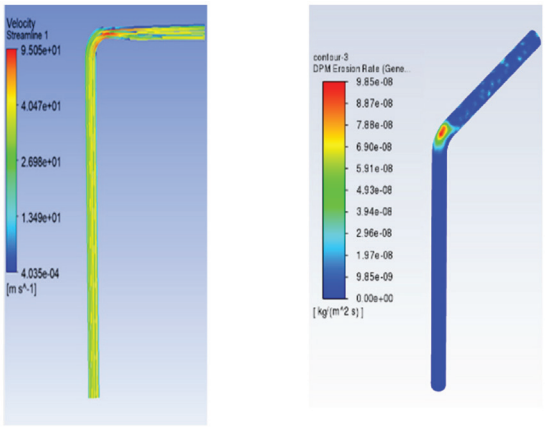

Fig. 9. Erosion rate plot and velocity plot at 200 µm particle size with swirling device (100rpm)

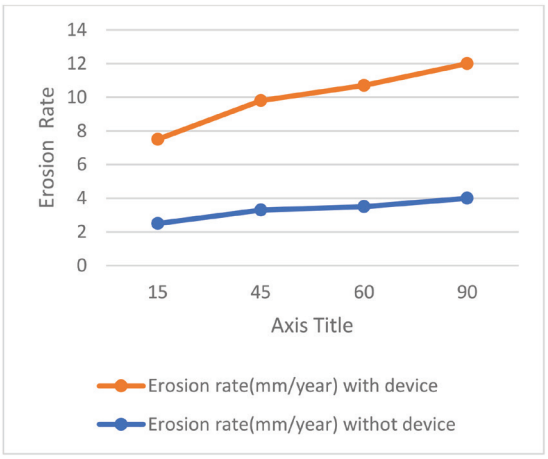

Graph 1. Erosion rate graph at different bend conditions

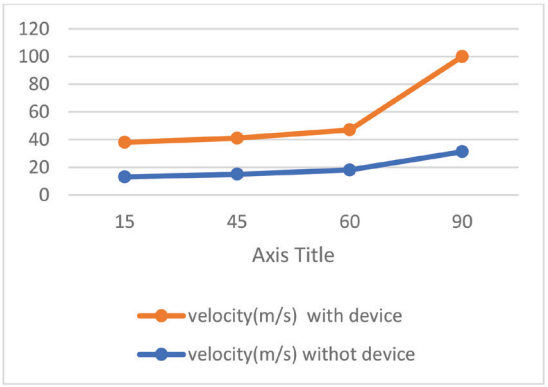

Graph 2. Velocity graph at different bend conditions

Erosion rate Graph: The erosion rate increases with increasing the bend angle of the sand pipe. The given graph shows the erosion rate at different bend angles in this study case-5 shows the Minimum erosion rate, and case-4 maximum erosion rate.

In the given study swirling device was not used in case-4. Due to this maximum erosion occurs. In case-5 swirling device with 100rpm was used for the study. so due to swirling devise erosion rate in case-5 decreased due to the swirling effect.

Velocity Graph: The velocity increases with increasing the rpm of the swirling device. The given graph shows the velocity at different bend angles. in this study case-8 shown maximum velocity rate, case-1 minimum velocity.

In the given study swirling device was not used in case-1 due to this minimum velocity occurs. In case-8 swirling device with 100rpm was used for the study. so due to swirling devise velocity in case-8 increases due to the swirling effect.

3. CONCLUSION

In this study, an erosion model based on Computational Fluid Dynamics (CFD) is employed to assess the erosion rate under different conditions, including pipe bend angle. Additionally, the study delves into the calculation of particle velocity and the investigation of pipe bend angle as part of the analysis. Based on the data in Table 3, the following conclusion can be reached:

- Figure 9 depicts the maximum erosion rates for a 90º bend without a swirling device.
- The higher erosion rate causes system failure and reduces the life cycle of the system.
- In the case of a 90º bend with a swirling device, it's observed that the maximum erosion rate decreases with swirling devices. This decrease in erosion rate is directly associated with an increase in the system's operational lifespan.
- In the absence of a swirling mechanism, when a particle strikes the L-tube wall, silica particles swirl. The highest velocity increase among the particles reaching the bend intrados is predicted to occur at the 90° bend.
- Then in this study swirling device is used to decrease the erosion rate. The swirling device swirls sand particles before hitting the pipe and reduces erosion rate.
- Erosion Rate decreases with less angle of bend due to less striking and swirling is very effective to reduce the bend erosion rate.
- Rotating of the particle by rotating part of the pipe work to minimize erosion rate.

4. FUTURE SCOPE

In our current study, we employ a swirling device to rotate particles and mitigate erosion effects, which has shown promise in reducing erosion rates. However, in future studies, we plan to replace this device with an automatic swirling device. This new device, driven by changes in air velocity, is expected to further enhance erosion rate reduction. The transition to automation is anticipated to offer benefits such as improved precision, consistency, and adaptability, potentially yielding significant advancements in erosion mitigation.

5. ACKNOWLEDGMENT

The faculty and supporting staff ofdesign center and CAD Centre Mechanical Engg, Department of DTU is acknowledged for providing Ansys Software workstation.

6. REFERENCES

1. ARUN, G., BABU, S. K., NATARAJAN, S. and KULASEKHARAN, N. (2020). *Numerical predictions of fluid dynamics and wall erosion characteristics in a circular 90 deg. pipe bend with single and multi-mittered joint.* Materials Today: Proceedings, *27*, 2109-2116.
2. LI, C., HUANG, Q., YAN, S. and HUANG, T. (2016). *Parametric CFD studies on erosion in the 3D double elbow*. International Journal of Engineering Systems Modelling and Simulation, 8(4), 264-272.
3. JIANG, F., LONG, Y., WANG, Y. J., LIU, Z. Z. and CHEN, C. G. (2015). *Numerical simulation of non-Newtonian core annular flow through rectangle return bends. Journal of Applied Fluid Mechanics*, *9*(1), 431-441.
4. RÖHRIG, R., JAKIRLIĆ, S. and TROPEA, C. (2015). *Comparative computational study of turbulent flow in a 90 pipe elbow*. International Journal of Heat and Fluid Flow, *55*, 120-131.
5. BANDYOPADHYAY, T. K. and DAS, S. K. (2013). *Non-Newtonian and gas-non–Newtonian liquid flow through elbows–CFD analysis.* Journal of Applied Fluid Mechanics, *6*(1), 131-141.
6. GHAZALI, M. F. and RAHIM, M. F. A. (2013). *CFD prediction of heat and fluid flow through U-bends using high Reynolds-number EVM and DSM models.* Procedia Engineering, 53, 600-606.
7. WANG, L., GAO, D. and ZHANG, Y. (2012). *Numerical simulation of turbulent flow of hydraulic oil through 90 circular-sectional bends*. Chinese Journal of Mechanical Engineering, *25*(5), 905-910.
8. ETEMAD, S., SUNDÉN, B. and DAUNIUS, O. (2006). *Turbulent flow and heat transfer in a square-sectioned U-bend. Progress in Computational Fluid Dynamics,* An International Journal, *6*(1-3), 89-100.
9. HOMICZ, G. F. (2004). *Computational Fluid Dynamic simulations of pipe elbow flow* (No. SAND2004-3467). Sandia National Laboratories

(SNL), Albuquerque, NM, and Livermore, CA (United States).

10. CHUNG, Y. M., TUCKER, P. G. and ROYCHOWDHURY, D. G. (2003). *Unsteady laminar flow and convective heat transfer in a sharp 180 bend.* International journal of heat and fluid flow, *24*(1), 67-76.
11. SONG B. and AMANO R.S. (2000). *Application of non-linear k-h model to a turbulent flow inside a sharp U-bend*, Comput. Mech. 26, 344–351.
12. SUDO, K., SUMIDA, M. and HIBARA, H. (2000). *Experimental investigation on turbulent flow through a circular-sectioned 180 bend. Experiments in Fluids*, *28*(1), 51-57.
13. FIEDLER, H. E. (1997). *A note on secondary flow in bends and bend combinations*. *Experiments in fluids*, *23*(3), 262-264.
14. HIROSHI Y, GENICHIRO K. and RYOTARO I, (1984). *Study on three-dimensional flow and heat transfer in Miter-Bend,* Bull. JSME 27 (231), 1905–1912.
15. HIROSHI Y, RYOTARO I and GENICHIRO K., (1987). *Fluid Flow and Heat Transfer in a Two-dimensional Miter-bend: Study of Unsteady Motion by Numerical Calculations: Heat Transfer, Combustion,* Power, *Thermophysical Properties*. JSME international journal: bulletin of the JSME, 30(259), 93-99.
16. DEAN, W. R., and HURST, J. M. (1959). *Note the motion of fluid in a curved pipe.* Mathematika, *6*(1), 77-85.